TASISpec - A Highly Efficient Multi-coincidence Spectrometer for Nuclear Structure Investigations of the Heaviest Nuclei

Andersson, L-L; Rudolph, Dirk; Golubev, Pavel; Herzberg, R-D; Hoischen, Robert; Merchan, E.; Ackermann, D.; Duellmann, Ch. E.; Eberhardt, K.; Even, J.; Gerl, J.; Hessberger, F. P.; Jaeger, E.; Khuyagbaatar, J.; Kojouharov, I.; Kratz, J. V.; Krier, J.; Kurz, N.; Prokopowicz, W.; Schaedel, M.; Schaffner, H.; Schausten, B.; Schimpf, E.; Semchenkov, A.; Tuerler, A.; Wollersheim, H-J; Yakushev, A.; Thoerle-Pospiech, P.; Hartmann, W.; Huebner, A.; Lommel, B.; Kindler, B.; Steiner, J.

Published in:
Nuclear Instruments & Methods in Physics Research. Section A: Accelerators, Spectrometers, Detectors, and Associated Equipment

DOI:
10.1016/j.nima.2010.06.243

2010

TASISpec – A Highly Efficient Multi-coincidence Spectrometer for Nuclear Structure Investigations of the Heaviest Nuclei

L.-L. Andersson[a], D. Rudolph[b], P. Golubev[b], R.-D. Herzberg[a], R. Hoischen[b,c], E. Merchán[b,c,d], D. Ackermann[c], Ch.E. Düllmann[c], K. Eberhardt[e], J. Even[e], J. Gerl[c], F.P. Heßberger[c], E. Jäger[c], J. Khuyagbaatar[c], I. Kojouharov[c], J.V. Kratz[e], J. Krier[c], N. Kurz[c], W. Prokopowicz[c], M. Schädel[c], H. Schaffner[c], B. Schausten[c], E. Schimpf[c], A. Semchenkov[f,g], A. Türler[f,h], H.-J. Wollersheim[c], A. Yakushev[f], P. Thörle-Pospiech[e], W. Hartmann[c], A. Hübner[c], B. Lommel[c], B. Kindler[c], J. Steiner[c]

[a] *University of Liverpool, Oliver Lodge Laboratory, Liverpool L69 7ZE, United Kingdom*
[b] *Lund University, S-22100 Lund, Sweden*
[c] *GSI Helmholtzzentrum für Schwerionenforschung GmbH, D-64291 Darmstadt, Germany*
[d] *Universidad Nacional de Colombia, Bogotá, Colombia*
[e] *Johannes Gutenberg-Universität Mainz, D-55128 Mainz, Germany*
[f] *Technische Universität München, D-85748 Garching, Germany*
[g] *University of Oslo, 0315 OSLO, Norway.*
[h] *Paul Scherrer Intitute, 5232 Villigen, Switzerland*

Abstract

TASISpec (*TA*SCA in *S*mall *I*mage mode *Spec*troscopy) combines composite Ge- and Si-detectors for a new detector setup aimed towards multi-coincidence γ-ray, X-ray, conversion electron, fission fragment, and α-particle spectroscopy of the heaviest nuclei. It exploits the TASCA separator's unique small image focal mode, i.e. the fact that evaporation residues produced in fusion-evaporation reactions can be focused into an area of less than 3 cm in diameter. This provides the possibility to pack detectors in very close geometry, resulting in an unprecedented detection efficiency of radioactive decays in prompt and delayed coincidence with implanted nuclei.

Key words: Recoil separators, Decay tagging spectrometer, Alpha, gamma-ray, and conversion electron spectroscopy at recoil separators, Si strip detector, Clover Ge detector, Cluster Ge detector
PACS: 23.60+e, 27.80.+w, 29.30.Dn, 29.30.Kv, 29.30.Ep, 29.40.Gx

1. Introduction

Experimental studies of very heavy or superheavy nuclei have challenged scientists for decades and the ability to produce new and heavier elements has continuously improved through the second half of the 20th century. For instance, the discovery of element $Z = 100$ was published in the 1950's [1], $Z = 105$ in the 1970's [2], $Z = 110$ in the 1990's [3], and $Z = 118$ – the heaviest element claimed so far – in the 2000's [4].

Ultimately the location of the theoretically predicted so called "island of stability" is sought [5, 6, 7, 8]. This region of more stable superheavy nuclei is predicted to exist in the vicinity of the next but yet experimentally unknown magic numbers of protons and neutrons. As an important stepping stone towards this region, theory predicted $^{270}_{108}Hs_{162}$ as a possible deformed doubly magic nucleus [9, 10, 11]. These predictions have been confirmed in recent years [12], providing an essential point of reference to further develop the theoretical predictions of the heaviest nuclei on route to the island of stability.

In order to keep up with the growing demand for experimental data on the heaviest elements, recoil separators have been built at different accelerator facilities around the world. These deal with the difficult task of separating the precious superheavy nuclei from the huge experimental background, as they are produced with cross sections of a few picobarn or less.

The existing recoil separators [13] can be divided into the vacuum type, which may comprise both electric and magnetic elements, and gas-filled types, which use only magnetic elements. Examples of existing vacuum separators used for superheavy element re-

Email address: lla@ns.ph.liv.ac.uk (L.-L. Andersson)

search are the Separator for Heavy-Ion reaction Products (SHIP) [14] at the GSI Helmholtzzentrum für Schwerionenforschung GmbH in Germany, the VASSILISSA separator [15] at the Flerov Laboratory for Nuclear Reactions in Russia, and the Fragment Mass Analyzer (FMA) [16] at the Argonne National Laboratory in the United States. Examples of gas-filled separators, on the other hand, are the Berkeley Gas-filled Separator (BGS) [17] at the Lawrence Berkeley National Laboratory in the United States, the Dubna Gas-filled Recoil Separator (DGFRS) [18] at the Flerov Laboratory for Nuclear Reactions, the Gas Filled Recoil Ion Separator (GARIS) [19, 20] at RIKEN in Japan, and the Recoil Ion Transport Unit (RITU) [21] in Jyväskylä, Finland. The TransActinide Separator and Chemistry Apparatus (TASCA) [22, 23] installed at the GSI Helmholtzzentrum für Schwerionenforschung GmbH has recently been added to the existing gas-filled separators. The commissioning of TASCA took place in 2006–2008, and the first scientific experiments were carried out in 2008 before TASCA entered the forefront of superheavy nuclei production in the year 2009 with element $Z = 114$ experiments [24, 25].

2. The TASCA Separator

TASCA is a gas-filled recoil separator specifically laid out for chemical and nuclear studies of elements with atomic numbers of 104 and larger. The construction was optimised for products from hot-fusion reactions like ^{238}U(^{48}Ca, $3n$)^{283}112 or ^{244}Pu(^{48}Ca, $3n$)^{289}114 [22]: The structure of the separator with one 30°-bending dipole magnet and two focusing quadrupole magnets (DQQ) allows for two different ion optical modes: the "High Transmission Mode" (HTM) and the "Small Image Mode" (SIM). The difference is the order of the horizontal and vertical focusing of the quadrupoles. HTM, which is the traditional focal mode in separators, is obtained via the DQ_hQ_v sequence. Here the indices indicate horizontal (h) and vertical (v) focusing. The DQ_vQ_h ordering leads to the SIM.

The HTM results in a horizontally elongated elliptically shaped image in the focal plane with a size of about 20 mm x 120 mm and a transmission of typically around 60% for superheavy element evaporation residues. The SIM on the other hand yields a near-circular shaped focal plane image. The image size is some 3 cm in diameter with a transmission through the separator of about 2/3 of the corresponding value in the HTM. For more details about TASCA, see Refs. [22, 23].

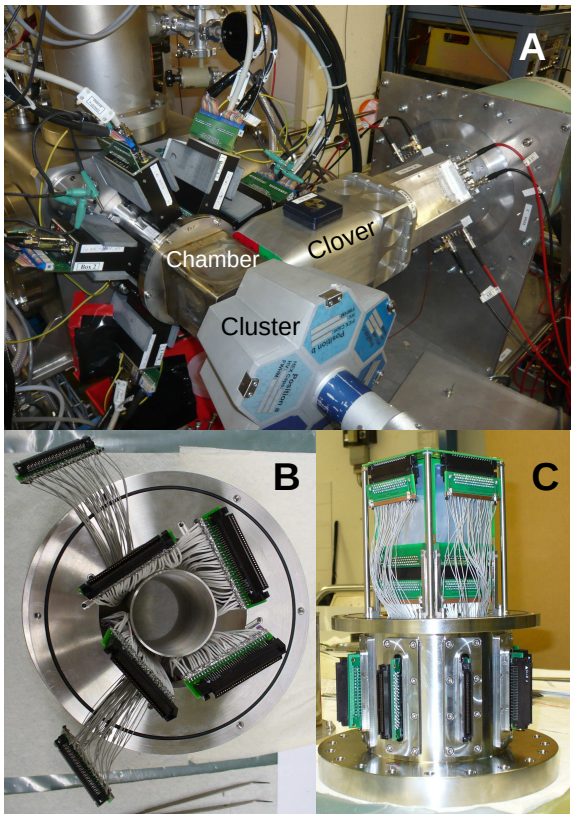

Figure 1: Panel A) A photograph of the commissioning set-up. The relative positions of the Ge-VEGA-clover and Ge-cluster detector in relation to the detector chamber is presented. Panel B) The internal structure of the feed-through tube with the recoil-transfer tube and the cables for the detectors. The four shorter cables are for the SSSSD and the two longer for the p- and n-side of the DSSSD. Panel C) The feed-through tube (bottom) with the connectors to the pre-amplifiers and the detector structure (top) is shown. Two of the SSSSD detectors are visible and so is the mounting of the two connectors for the DSSSD.

3. Detection Setup

TASISpec combines double-sided (DSSSD) and single-sided (SSSSD) Si-strip detectors with composite Ge detectors. The underlying philosophy is to provide a compact inner Si-detector section, which should be as transparent as possible for low-energy γ rays or X-rays. The setup can be seen in Fig. 1A. In this photograph, the upper left-hand corner shows the rear chamber of the TASCA separator. At the very end of this chamber is the TASISpec feed-through tube and detector chamber positioned. The photograph shows four of the six pre-amplifiers for the Si-detectors as they are positioned around the feed-through tube. The tube itself has an inner diameter of 90 mm and it contains the cables from the Si-detectors as well as a recoil-transfer tube with an inner diameter of 50 mm, as can be seen in

Fig. 1B. Evaporation residues separated in TASCA will pass through this inner tube to enter the detection area. The small space between the inside of the outer tube and the outside of the inner tube also houses the connectors which feed the detector signals through from the low-pressure gas filling inside TASCA to the preamplifiers positioned in air. These PCB-board based feedthroughs and attached high-density connectors are visible in the lower part of Fig. 1C.

The construction with the feed-through tube followed by the detector chamber on top is illustrated in its full length of 260 mm in Fig. 1C. When placing this structure behind the TASCA separator it forms an extension. The extension is as short as possible to allow for an easy mounting and dismounting of TASISpec, and it is also essential to gain the required space for a compact arrangement of the surrounding composite Ge-detectors. The placement of one former Euroball Cluster [26, 27] and one VEGA-Clover [28] Ge-detector used in the commissioning setup can be seen in Fig. 1A.

3.1. Si-detectors

In total, there are five Si detectors in the experimental setup. Four of these are SSSSDs and one is a DSSSD.

The DSSSD is used as the implantation detector. It is a 32 $\times$ 32 strip detector with an active area of 58 mm $\times$ 58 mm. Each strip is separated from the neighbouring ones via an inactive area of 60 μm. Detectors with thicknesses of 0.31, 0.52, or 1.0 mm are available, while for the commissioning the DSSSD was 0.31 mm thick. Upstream from the DSSSD, the four 60 mm $\times$ 60 mm active area, 32-strip SSSSDs with a thickness of 1.0 mm are placed. The strips of the SSSSDs are oriented along the beam axis. The four detectors complete the cube-like inner structure which has an inner cube-side length of 65 mm. One face of the cube is left open for the incoming particles. The structure of the detector cube is visualised in Fig. 1C, where two of the SSSSD are seen. The Si-cube is used for the registration of implanted recoils, and the detection of subsequent α particles, conversion electrons, and fission fragments. In the following the four SSSSDs will be referred to as the "box".

Using the geometrical constraints and assuming that a nucleus is implanted at the very centre of the DSSSD one obtains an estimated geometrical Si-detector coverage of 81% for this detector setup. Whilst fission fragments are detected within the DSSSD with an essentially 100% efficiency, α particles and conversion electrons are expected to be detected with a total efficiency similar to this geometrical detector coverage. Note that about 4% of the geometrical coverage is lost due to inactive areas around the edges of the detectors while the remaining 15% are lost due to the one side of the detector cube which is kept open for incoming evaporation residues.

The five Si detectors are positioned inside a detector chamber, the first version of which can be seen in Fig. 1A. This chamber is welded together from pieces of stainless steel. The five walls – which are facing the Ge-detectors – are 0.5 mm thin to minimise the energy loss and the scattering of the γ-rays on their way to the Ge-detectors. To assure mechanical stability of the structure, the thin walls were welded onto a thicker stainless-steel skeleton. Each outer side of the skeleton is 108 mm wide. This detector chamber was used for the first commissioning phase, including the data presented here.

In the course of further developments, a second chamber has been produced, milled out of a single piece of aluminium. The nominal wall thickness of 3.0 mm is reduced to 1.5 mm in circles of 85 mm diameter on each of the five cube sides facing Ge-detectors. In addition, the outer dimensions of the aluminium chamber were reduced to 103 mm on two sides, while kept at 108 mm on the remaining two sides. This means that the cube is slightly off-centre to accommodate the two DSSSD connectors (cf. Fig. 1C).

Another improvement in the course of the commissioning phase concerns the positioning of the DSSSD connectors. In the first version, displayed in Fig. 1C, they shadow a considerable fraction of the subsequent Ge-clover detector. Therefore, a revised PCB design for the DSSSD foresees a direct coupling to ultra-thin coaxial cables with DSSSD connector placements at the same height as the ones for the SSSSD, i.e. out of sight for γ rays travelling from the DSSSD towards the Ge-clover detectors. This is expected to further increase the low-energy γ-ray efficiency by a few percent.

3.2. Ge-detectors

A total of five Ge-detectors will be included in the final experimental setup. Four of these are of the four-crystal so-called "clover" type [29]: two Ge-VEGA-clovers [28], one SHIP Ge-clover [30] and one resembling those used in the former Euroball array [27, 31]. Each of the four Ge-clovers will be placed behind one of the four SSSSD's. The fifth Ge detector is placed behind the DSSSD. This detector is of the seven-crystal "cluster" type [26, 27] and it also originates from the former Euroball array. This means that in total $4 \times 4 + 7 = 23$ Ge-crystals will be included in TASISpec.

The Ge detectors are placed as close as possible around the detector chamber. This assures that the distance from the Si-wafers to the Ge-crystals is minimised. Due to the small size of the Si-detector chamber in comparison to the front faces of the Ge-detectors, there will even be an overlap between their positions at the cube edges. This is especially true for the front face of the cluster detector. This compact setup of 23 Ge crystals will allow for both high overall detection efficiency and moreover high γ-γ or γ-X-ray coincidence probabilities, including several options for add-back schemes, allowing for a partial reconstruction of γ-rays scattering from one crystal into another.

3.3. The Time-of-flight Detector

In 2009, a time-of-flight detector was installed into the standard TASCA focal-plane chamber, some 50 cm upstream from the focal plane of TASISpec. This detector is a multi-wire proportional counter (MWPC), similar to the one described in Ref. [32].

As ions pass through this detector they generate a signal. This means that if a signal in the MWPC is registered in coincidence with a signal in the DSSSD it will be identified as a particle having passed through the separator and being focussed onto the DSSSD. However, if the DSSSD signal is in anti-coincidence with the MWPC it will be identified as a radioactive decay of a nucleus which is already implanted into the DSSSD.

3.4. Electronics & DAQ

Analogue signals from the DSSSD and the SSSSDs are transmitted inside the TASISpec detector chamber to the feed-throughs by means of ultra thin (0.62 mm in diameter) 50-Ω coaxial cables; specification number DAS501, produced by Junkosha Inc., Japan. Immediately on the air side of the feedthrough connectors the signals are processed by state-of-the-art low noise front-end electronics (FEE), namely charge sensitive multichannel CSP_07 preamplifiers developed at the University of Cologne [33]. To assure noise minimisation and optimum energy resolution, the signals from the preamplifier outputs are transmitted in differential form via shielded cables to commercially available STM-16+ shaping and timing filter amplifiers [34]. The energy and timing output of the STM-16+ were digitised by means of standard VME ADC and TDC modules, and readout by the generic GSI data acquisition system, MBS [35, 36].

Two dynamic ranges were implemented for the p-side of the DSSSD. The preamplifier output signals of these 32 strips were split into two branches to record both α particles (ADC range 0-20 MeV) and fission products (ADC range 0-200 MeV). The ADC range of the n-side of the DSSSD was set to 0-40 MeV, while all four box detector read-outs were running in a 0-20 MeV range. For a given experiment these ranges can be easily adjusted by changing the amplification of the signals in the STM-16+ modules. The preamplifier outputs of the Ge-detectors are processed and digitised by VME-based sampling ADCs.

The STM-16+ trigger outputs as well as Ge-detector's FEE trigger signals were processed in standard NIM electronics to generate master triggers and required control signals for the data acquisition system.

A variety of hardware triggers were incorporated in the detection system. The triggers provide the possibility to use one or several at the same time. The trigger conditions used during the commissioning experiments are listed in Tab. 1.

Table 1: Hardware trigger conditions in the electronics setup.

Trigger	Condition
1	DSSSD OR
2	box AND DSSSD
3	box OR
4	box AND γ
5	DSSSD AND γ
6a	γ OR
6b	γ-γ

4. Commissioning Experiments

To explore the properties of the detector setup, commissioning experiments were run using two different beams, ^{48}Ca and ^{64}Ni, and a series of target materials. Whilst some of the reactions were run merely to test beam target combinations and measure the TASCA transmissions, the results from the ^{206}Pb(^{48}Ca,2n)^{252}No and ^{207}Pb(^{48}Ca,2n)^{253}No reactions have been used to explore the properties of TASISpec in more detail.

4.1. Experimental Efficiencies

The efficiency of the Si detectors has been estimated using the experimental results from the ^{207}Pb(^{48}Ca,2n)^{253}No reaction. As the residues are implanted a few micrometers into the DSSSD, it is obvious (simply from the geometry) that about 50% of the emitted α particles are detected within the DSSSD. These α particles will hence deposit their full energy in the detector. The remaining 50% will be emitted in backward

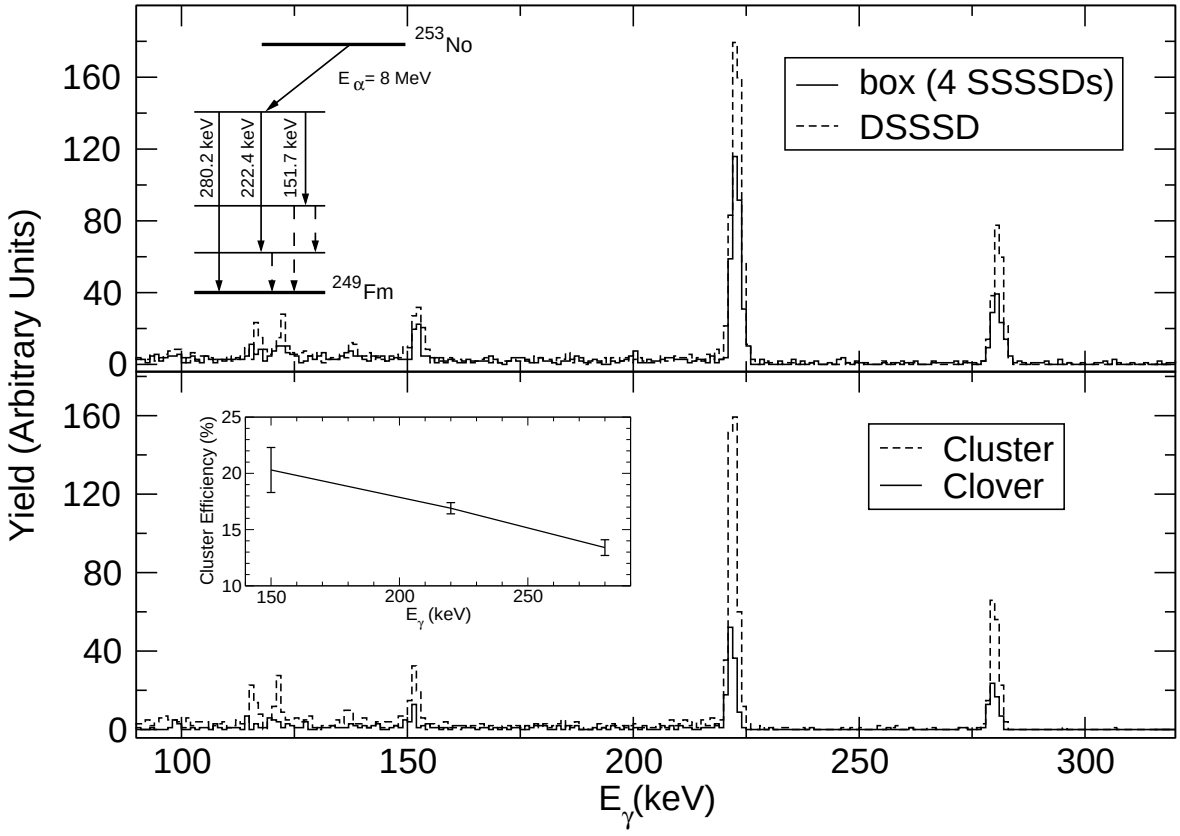

Figure 2: Gamma-ray spectra taken in coincidence with α particles corresponding to the decay of ^{253}No. In the upper left corner a sketch of the α decay of the ground state of ^{253}No and the subsequently emitted γ-rays is given. Upper panel: Relative efficiencies of the Si detectors illustrated via the spectra of γ rays detected in coincidence with α particles. For the α particles detected in the Si-detector "box" the correlated γ-ray spectrum is indicated by a solid line and for those detected in coincidence with the α particle detected in the DSSSD the spectrum is indicated in a broken line. Lower panel: The broken line spectrum is obtained when the γ rays are detected in the seven-crystal Ge-cluster detector and the spectrum indicated by a solid line when they are detected in the four-crystal Ge-VEGA-clover detector, both with the α particle detected in the DSSSD. The insert shows how the efficiency for the cluster detector varies as a function of γ-ray energy. See text for details.

angles. This means that they deposit some energy in the DSSSD and then *(i)* deposit their remaining energy in either of the four single sided Si detectors, or *(ii)* escape detection by exiting the detector "box" with an angle close to 180° relative to the beam axis. While case *(i)* means that the α particles may still be identified, case *(ii)* means that the α particle is lost. It should be noted, however, that the α particles detected in the SSSSD's have lost somewhat different amounts of energy in the dead layers of the double- and single-sided Si detectors depending on their angle of emission.

The upper panel of Fig. 2 illustrates the relative intensities of γ rays detected in coincidence with α particles detected in the DSSSD (indicated by a broken line). These α particles are detected with their full energy (between 8.0-8.4 MeV), see Fig. 3. The spectrum in Fig. 2 also shows α particles detected in the SSSSD (indicated by a solid line). These include all the α particles which are not fully detected in the DSSSD. These particles have to be registered with an energy loss of 0.3-8.0 MeV in either of the SSSSD strips and simultaneously having deposited an energy greater than zero in the *p*-side of the DSSSD. Their total detected energy will vary depending on the angle at which they travel though the dead layers of the DSSSD and SSSSD. The requirement of an α-γ coincidence excludes all α particles in the decay chain except the ones originating from the ^{253}No decay. An estimate of the efficiency in the box can then be obtained by comparing the number of detected γ rays in the two spectra. The number of detected α particles in the box is 60(3)% of what is detected in the DSSSD. Thus, under the assumption that 50% of the α particles are detected in the DSSSD, one can deduce that 30(2)% of the α particles are detected

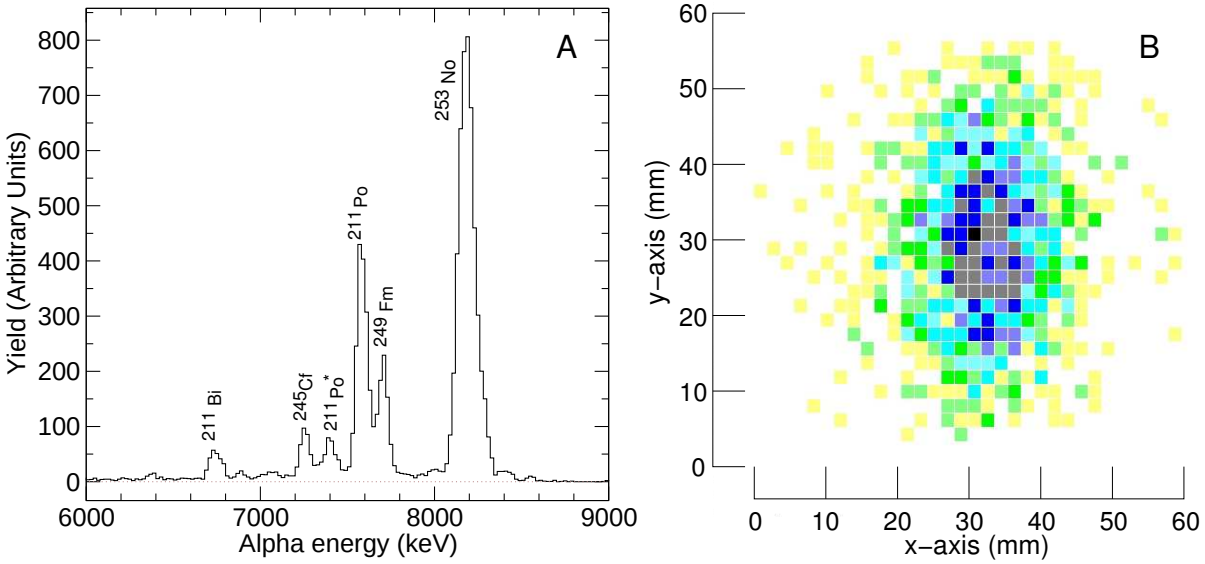

Figure 3: Detected α particles in the DSSSD for the ^{48}Ca+^{207}Pb run (panel A). Note that the spectrum is calibrated using an external source resulting in an offset in the detected energy of around +100 keV. Panel B) The position of the α particles detected in the DSSSD with an energy of 8.0-8.4 MeV, correlated with ^{253}No. Using the magnetic settings, the image size is here adjusted to form a even distribution over the full detector size, i.e. the image size is slightly larger than what TASCA can achieve. On the *x* and *y*-axis the size of the DSSSD is indicated in millimetres.

in the "box". This means that in total 80(2)% of the emitted α particles will be detected using the TASISpec Si-cube. Thus, the efficiency obtained when using a realistic extended position distribution is in line with the single point geometrical estimation in Sec. 3.1.

In the commissioning setup the Ge cluster detector, and one of the Ge VEGA-clover detectors were used. The two detectors have been used to determine the γ-ray efficiencies in the setup. In a similar manner as above, the α particles have been correlated with the detected γ rays. The number of detected α - γ coincidences where the α particles are detected in the DSSSD and the γ ray in either the clover or the cluster detector has been put in relation to the number of detected α particles in the DSSSD. The correlation is made via the α particle of 8.0-8.4 MeV which is emitted in the decay from the ground state of ^{253}No into the excited 280 keV state in ^{249}Fm followed by either of three γ-rays with energies measured in the present study at 151.7, 222.4, and 280.2 keV. A sketch of the decay scheme [30] can be found in Fig. 2.

In the lower panel of Fig. 2 the resulting spectra from the two Ge-detectors are shown. The number of detected γ-ray quanta obtained from these spectra are corrected for internal conversion. This correction uses the internal conversion coefficient, α_{tot} = 0.212(3), 0.0910(13), and 0.0554(8) [37] for the 151.7, 222.4, and 280.2 keV transitions, respectively. The latter assumes that they are all $E1$ transitions [30, 38] and that the uncertainty of the γ-ray energies is 1 keV. From these calculations, the average γ-ray efficiency using all three transitions was found to be 16.3(5)% for the cluster detector and 4.7(2)% for the clover at an average γ-ray energy of around 220 keV. Naturally, this efficiency varies as a function of energy. In Fig. 2 the inserted graph shows how the efficiency varies in the Ge-cluster detector for the three γ-ray energies. The calculations utilises the relative intensity I_{rel} = 0.18(1) : 1 : 0.48(2) [30] for the 151.7, 222.4, and 280.2 keV transitions, respectively.

It should be noted that the efficiencies to some extent reflect the fact that the geometrical efficiency, i.e. the size of the front face of the Ge-cluster detector is larger than for the Ge-clover detector. Furthermore, the clover detector used in the commissioning setup was placed behind one of the two SSSSD, which have a connector from the DSSSD behind it (cf. Fig. 1C and Sec. 3.1). Thus, the present γ-ray efficiency is slightly reduced by the extra material between the Si detector and the Ge crystals in comparison to the two "connector free" de-

tectors.

4.2. Energies in the DSSSD

Concentrating on the energies detected in the DSSSD, a few features of the detection setup are worth noting.

The spectrum of the α particles detected during the beam-off period of the pulsed beam in the ^{48}Ca + ^{207}Pb reaction is shown in Fig 3A. Clearly, the ^{253}No nucleus and its daughter products following in the decay chain are dominating the spectrum. The α chain includes the three particles in the decay sequence: ^{253}No $\rightarrow$ ^{249}Fm $\rightarrow$ ^{245}Cf $\rightarrow$ ^{241}Cm. Note that for the spectrum in Fig. 3A the detector was calibrated using an external source. This causes an offset in energy of some 100 keV originating from the fact that an α particle emitted from a nucleus placed in front of the detector – such as a calibration source – is losing energy when entering the active detector material through the dead layer of the Si detector. If the α particle instead is emitted from a mother nucleus which is already implanted into the detector no such energy loss takes place. Furthermore, if an implanted nucleus is α decaying the recoil energy of the nucleus itself will also be detected in the same pixel as the α particle. Both effects will result in an overestimation of the energy of the α particle.

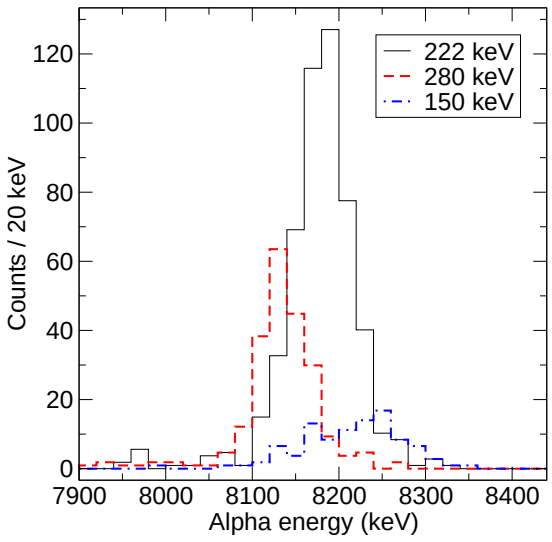

Figure 4: The summing of α particle and conversion electron energies in the DSSSD. Selecting α particles in coincidence with one of the three γ rays in ^{253}No results in different positions of the registered "Si-energy". This effect has been discussed previously in, for instance, Ref. [30].

In Fig. 3B the hitpattern as seen in the DSSSD is shown. This hitpattern shows the pixels in which the 8.0-8.4 MeV α particles (relating to the decay of the ground state of ^{253}No) have been detected. More than 90% of the events lie within a 20 mm $\times$ 30 mm small area, in line with the expected result for the SIM focusing mode of TASCA [22].

Another feature can be noted when the α decay is promptly followed by a conversion electron (CE). If the two particles are emitted within a very short period of time, the detector pulses from the α particle and the electron will add up, leading to a shift of the measured α-particle energy [39]. In the case of ^{253}No the α decay populates an excited level at E*=280 keV in the daughter nucleus. The detected energy of the α-particle will thus be influenced by CE originating from the decay of this level and from levels populated in the decay of it (see Fig. 2). The total energy in a pixel thus equals the energy of the α particle plus some energy originating from the CE. Ideally the extra energy would originate from the energy of the state minus the binding energy of the electron. In reality the vacancy in a given atomic shell (K, L, M, ...) can be followed by vacancies in higher shells giving rise to low energy X-rays and Auger electrons which also may be detected in the DSSSD pixel. As a rule of thumb the detected energy following a CE is given by:

$$E \approx E_T - \frac{1}{2}E_{B.E.} \quad (1)$$

where E_T is the transition energy and $E_{B.E.}$ is the binding energy of the L-shell if the energy of the state is small – which is the case in the transitions discussed here – and hence not large enough to overcome the binding energy of the K-electrons. In the case of Nobelium isotopes, the binding energies of the K and L shells are $E^K_{B.E.}$=149.2 keV, $E^{L_1}_{B.E.}$=29.2 keV, $E^{L_2}_{B.E.}$=28.3 keV, $E^{L_3}_{B.E.}$=21.9 keV [46].

As seen in the decay scheme in Fig. 2 the α decay in ^{253}No can be followed by either *(i)* a 280 keV transition into the ground state of ^{249}Fm, *(ii)* a 222 keV transition followed by a 58 keV transition [α_{tot} = 51.9(8) [37]] which, as can be seen from the large conversion coefficient for this transition, can be replaced with an internal conversion electron, or *(iii)* a 151 keV transition followed by either a 129 keV transition [α_{tot} = 8.40(13) [37]] or by a 71 keV transition [α_{tot} = 28.8(5) [37]], which is followed by the 58 keV transition discussed above. Either of these transitions is highly converted. The corresponding CE may either be stopped in the DSSSD or escape after some loss of energy. The effect of energy summing can be seen if comparing the apparent α energies in coincidence with the three γ transitions as shown in Fig. 4. In case of

the 222 keV line accompanied by CE from the 57 keV $9/2^+ \rightarrow 7/2^+$ transition an energy shift compared to α particles coincident with the 280 keV transition into the ground state can be observed. In the case of the 151 keV transition, the $11/2^+$ level populated by it, rather decays via two M1 transitions $11/2^+ \rightarrow 9/2^+ \rightarrow 7/2^+$ into the ground state than by a single E2 transition $11/2^+ \rightarrow 7/2^+$. So four possibilities have to be considered: both CE escape the detector, both CE are fully stopped in the detector, either one of the CEs is stopped while the other escapes (note that the CE have different energies). This leads not only to a shift in the energy but also to a significant broadening of the peak.

4.3. The Decay of ^{252}No

The half-life of the ground-state of ^{252}No is well known from several publications: $T_{1/2}$ = 2.4(2) s [40], $T_{1/2}$ = 2.3(2) s [41], $T_{1/2} = 2.4^{+0.5}_{-0.4}$ s [42], $T_{1/2} = 2.25^{+0.18}_{-0.16}$ s [43], and $T_{1/2}$ = 2.4(3) s [44]. In the present analysis, a double exponential fit has been used and a value of $T_{1/2}$ = 2.51(24) s was obtained using the events from spontaneous fission and α decay, always position correlated within the same DSSSD pixel with a preceding recoil implantation signal of proper energy. The implant is here identified with an energy range of 14-21 MeV during the beam on period, fission is identified with an energy exceeding 100 MeV during the beam off period and the ^{252}No α particles are selected in an energy range of 8.3-8.5 MeV during beam off.

The present half-life agrees with the previous measurements. Furthermore, the half life of the two decay processes have been explored separately as was done previously in Ref. [45]. The previous publication obtained half lives of $T_{1/2}$ = 2.54(7) s for the spontaneous fission and $T_{1/2}$ = 2.46(5) s for the α decay. In the current analysis, the results are illustrated in Fig. 5 and amount to $T_{1/2}$ = 2.24(46) s for the fission and $T_{1/2}$ = 2.43(30) s for the α decay. Furthermore, the branching ratio of α-decay/fission/electron capture has previously been explored and determined as 24(4)%/74.8(40)%/<1.6% [44] meaning the percentage of α decays in relation to (fission+alpha) is 24.3(43)%. In the current analysis the corresponding result is 21.6(20)%, which within errors agrees well with the previous value.

Time correlations between the α decays of ^{252}No and ^{248}Fm have also been studied. The half life of ^{248}Fm has previously been measured to $T_{1/2}$ = 36(3) s [46] and $T_{1/2}$ = 31.6(42)s [47]. In the current analysis, the obtained half life is $T_{1/2}$ = 38.7(69) s.

These results show that implantation-decay correlation times in the order of a minute can easily be obtained with TASISpec though the number of pixels is not exceedingly high compared with other implantation set-ups [48, 49].

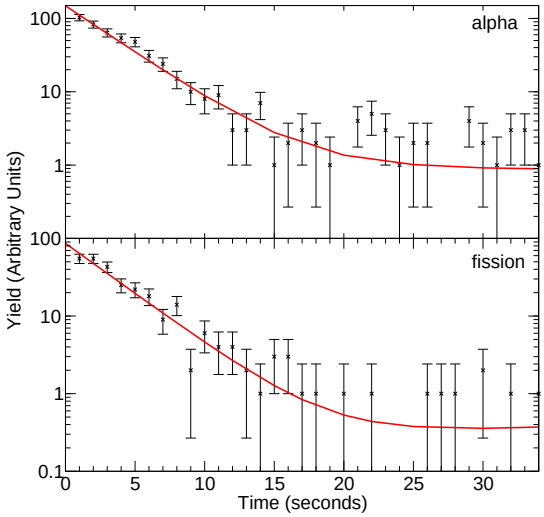

Figure 5: The decay of the ground state of ^{252}No. The upper panel shows α decays with a half life of $T_{1/2}$ = 2.40(17) s. The lower panel shows spontaneous fission where the half life of $T_{1/2}$ = 2.33(21) s was obtained.

5. Summary and Outlook

The very successful commissioning runs will now be followed by main beam experiments and the setup is under permanent development and improvement.

For instance, the potential benefits gained from the usage of pulse-shape electronics for the DSSSD are currently being explored. The advantage would be the possibility to separate ionisation paths in the Si detectors originating from different incidenting particle types.

Acknowledgements

We would like to thank Gammapool for the use of the cluster Ge-detector. Also our gratitude goes to the ECR ion source and UNILAC staff for providing excellent and stable ^{48}Ca beams and to the supporting staff at GSI for their invaluable support and efforts.

References

[1] A. Ghiorso *et al.*, Phys. Rev. **99**, 1048 (1955).
[2] G. N. Flerov *et al.*, Nucl. Phys. A **160**, 181 (1971).
[3] S. Hofmann *et al.*, Z. Phys. A **350**, 277 (1995).
[4] Yu. Ts. Oganessian *et al.*, Phys. Rev. C **74**, 044602 (2006).
[5] S. G. Nilsson *et al.*, Nucl. Phys. A **115**, 545 (1968).

[6] E. D. Fiset and J. R. Nix, Nucl. Phys. A **193**, 647 (1972).
[7] Yu. Ts. Oganissian, Phys. Atom. Nucl., **63**, 1315 (2000).
[8] M. A. Stoyer Nature **442**, 876 (2006).
[9] Z. Patyk, A. Sobiczewski, and S. Cwiok, Nucl. Phys. A **502**, 591 (1989).
[10] Z. Patyk and A. Sobiczewski, Nucl. Phys. A **533**, 132 (1991).
[11] M. Bender, P.-H. Heenen, and P.-G. Reinhard, Rev. Mod. Phys. **75**, 121 (2003).
[12] J. Dvorak *et al.*, Phys. Rev. Lett. **97** 242501 (2006).
[13] Ch. E. Düllmann, Nucl. Instrum. Meth. B **266** 4123 (2008).
[14] G. Münzenberg *et al.*, Nucl. Instrum. Meth. **161**, 65 (1979).
[15] A. V. Yeremin *et al.*, Nucl. Instrum. Meth. A **274** 528 (1989).
[16] C. N. Davids *et al.*, Nucl. Instrum. Meth. B **70**, 358 (1992).
[17] K. E. Gregorich *et al.*, Phys. Rev. C **72**, 014605 (2005).
[18] K. Subotic *et al.*, Nucl. Instrum. Meth. A **481** 71 (2002).
[19] K. Morita *et al.*, Nucl. Instrum. Meth. B **70** 220 (1992).
[20] K. Morita *et al.*, Eur. Phys. J. A **21** 257 (2004).
[21] M. Leino *et al.*, Nucl. Instrum. Meth. B **99** 653 (1995).
[22] A. Semchenkov *et al.*, Nucl. Instrum. Meth. Phys. Res. B **266**, 4153 (2008).
[23] M. Schädel, Eur. Phys. J. D **45**, 67 (2007).
[24] Ch. E. Düllmann *et al.*, submitted to Phys. Rev. Lett. (E114)
[25] A. Yakushev *et al.*, in preparation.
[26] J. Eberth *et al.*, Nucl. Instrum. Meth. A **369**, 135 (1996).
[27] J. Simpson, Z. Phys. A **358**, 139 (1997).
[28] J. Gerl, H. Grawe, E. Roeckl, H. J. Wollersheim, VEGA a proposal for Versatile and Efficient Gamma-detectors, GSI Darmstadt, Report, 1998.
[29] G. Duchêne *et al.*, Nucl. Instrum. Meth. A **432**, 90 (1999).
[30] F. P. Heßberger *et al.*, Eur. Phys. J. A **22**, 417 (2004).
[31] F. A. Beck, "Proceedings of the Conference on Physics from Large γ-ray Detector Arrays", Berkeley, LBL 35687, CONF 940888, UC 413, 1994, p. 154.
[32] K.E. Gregorich *et al.*, Eur. Phys. J. A **18**, 633 (2003).
[33] G. Paskovoci, IKP, Cologne, private communications.
[34] `http://www.mesytec.de`
[35] `http://www-wnt.gsi.de/daq/`
[36] H. G. Essel and N. Kurz, "The general purpose data acquisition system MBS", IEEE Trans. Nucl. Sci. , **47**, no. 2, pp. 337, April 2000.
[37] T. Kibédi, T. W. Burrows, M. B. Trzhaskovskaya, P. M. Davidson, C. W. Nestor Jr ., Nucl. Instr. and Meth. A **589** 202 (2008).
[38] R.-D. Herzberg, J. Phys. G: Nucl. Part. Phys. **30**, R123 (2004).
[39] F. P. Heßberger et al., Nucl. Instrum. Meth. A **274**, 522 (1989).
[40] Y. T. Oganessian, Sov. J. At. Energy **28**, 502 (1970).
[41] C. E. Bemis jr *et al.*, Phys. Rev. C **15**, 705 (1977).
[42] F. P. Heßberger et al., J. Less-Common Met. **122**, 445 (1986); F. P. Heßberger, GSI Report GSI-85-11, 1985.
[43] Yu. A. Lazarev *et al.*, Phys. Scr. **39**, 422 (1989).
[44] R.-D. Herzberg *et al.*, Phys. Rev. C **65**, 014303 (2001).
[45] A. P. Leppänen *et al.*, Eur. Phys. J. A **28**, 301 (2006).
[46] R. B. Firestone, V. S. Shirley, C. M. Baglin, S. Y. F. Chu and J. Zipkin, Table of Isotopes (eighth ed.), Wiley, New York (1996).
[47] K. Nishio *et al.*, Physics of Atomic Nuclei **69**, 1399 (2006).
[48] R. D. Page *et al.* Nucl. Instrum. Meth. B **204**, 634 (2003).
[49] K. Hauschild *et al.* Nucl. Instrum. Meth. A **560**, 338 (2006).